Chemical-Shift-Perturbation Mapping of the Phosphotransfer and Catalytic Domain Interaction in the Histidine Autokinase CheA from *Thermotoga maritima*[†,‡]

Damon J. Hamel,[§] Hongjun Zhou,[§] Mary R. Starich,[||] R. Andrew Byrd,[||] and Frederick W. Dahlquist*[,§]

Department of Chemistry and Biochemistry, University of California−Santa Barbara, Santa Barbara, California 93106, and Structural Biophysics Laboratory, National Cancer Institute at Frederick, Post Office Box B, Frederick, Maryland 21701

Received April 24, 2006; Revised Manuscript Received June 2, 2006

ABSTRACT: Regulating the activity of the histidine autokinase CheA is a central step in bacterial chemotaxis. The CheA autophosphorylation reaction minimally involves two CheA domains, denoted P1 and P4. The kinase domain (P4) binds adenosine triphosphate (ATP) and orients the γ phosphate for phosphotransfer to a reactive histidine on the phosphoacceptor domain (P1). Three-dimensional triple-resonance experiments allowed sequential assignments of backbone nuclei from P1 and P4 domains as well as the P4 assignments within a larger construct, P3P4, which includes the dimerization domain P3. We have used nuclear magnetic resonance chemical-shift-perturbation mapping to define the interaction of P1 and P3P4 from the hyperthermophile *Thermotoga maritima*. The observed chemical-shift changes in P1 upon binding suggest that the P1 domain is bound by interactions on the side opposite the histidine that is phosphorylated. The observed shifts in P3P4 upon P1 binding suggest that P1 is bound at a site distinct from the catalytic site on P4. These results argue that the P1 domain is not bound in a mode that leads to productive phosphate transfer from ATP at the catalytic site and imply the presence of multiple binding modes. The binding mode observed may be regulatory or it may reflect the binding mode needed for effective transfer of the histidyl phosphate of P1 to the substrate proteins CheY and CheB. In either case, this work describes the first direct observation of the interaction between P1 and P4 in CheA.

In bacteria, two-component signal-transduction systems are predominantly mediated by histidine kinases. These two-component systems regulate many processes essential to cell viability, including but not limited to gene expression, sporulation, microbial pathogenesis, and chemotaxis (*1*−*5*). Additionally, protein histidine kinases are ubiquitous in prokaryotes, while homologues in higher lifeforms are rare. This discrepancy makes them attractive targets for novel antibiotic compounds, and hence, their regulatory mechanisms are of significant interest.

In bacterial chemotaxis, a well-studied cast of proteins form a network capable of measuring temporal concentration changes in extracellular chemical stimuli and regulating the swimming behavior of the cell accordingly. During chemotaxis, bacteria alternate between two swimming modes. The first, commonly referred to as smooth swimming, is achieved by the counterclockwise rotation of flagella. The second mode, commonly referred to as a tumble, is initiated by reversal of the sense of rotation to clockwise. In the absence of attractant or repellent gradients, bacteria travel in a random "walk" with no net displacement over time. In the presence of such gradients, bacteria modulate their swimming behavior to suppress tumbles when swimming in a favorable direction. Over time, the net result of this modulation of flagellar rotation is migration toward the more favorable environment.

Three intermediate chemotaxis proteins define the pathway followed in the propagation of the signal from the transmembrane receptors to the flagellar motors. The receptor coupling protein, CheW, forms a necessary interface between the receptor and the protein histidine kinase, CheA. The signal transducer CheA autophosphorylates at a rate controlled by the signaling state of bound receptors. Once phosphorylated, CheA quickly transfers the phosphate group to the response regulators CheB and CheY. While CheB removes methyl esters from the receptor, CheY diffuses throughout the cell to transiently interact with the flagellar motors. Ultimately, the flagellar motor complex reacts to the binding of phosphorylated CheY by changing the probability of reversing its rotational direction.

The CheA proteins from all known organisms are made up of five modular domains, labeled P1−P5, with each being responsible for specific functions (*6*) (Figure 1). The N-terminal P1 domain contains a conserved histidine residue responsible for accepting a γ-phosphoryl group from adenosine triphosphate (ATP)[1] and subsequently transferring it to CheY or other response regulator domains. P2 binds CheY, thus increasing the effective local concentration of CheY. The P1 and P2 domains are separated from each other

[†] This work was funded by NIH Grant 5R01GM059544-25.

[‡] NMR assignments have been submitted to the BioMagResBank, accession numbers 7132 and 7133.

* To whom correspondence should be addressed. E-mail: dahlquist@chem.ucsb.edu. Telephone: (805) 893-5326. Fax: (805) 893-4120.

[§] University of California−Santa Barbara.

[||] National Cancer Institute at Frederick.

[1] Abbreviations: ATP, adenosine triphosphate; ADPCP, 5′-adenyl-(β,γ-methylene)-diphosphonate; DTT, dithiothreitol; EDTA, ethylenediaminetetraacetic acid; F-5-M, fluorescein-5-maleimide; NMR, nuclear magnetic resonance; Tris, hydroxymethylaminoethane; TROSY, transverse relaxation optimized spectroscopy; WT, wild type.

10.1021/bi060798k CCC: $33.50
Published on Web 07/13/2006

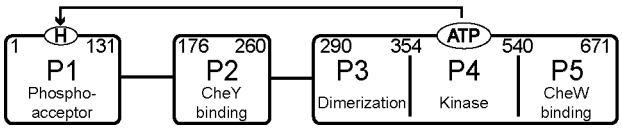

FIGURE 1: Histidine kinase CheA. Numbers represent the range of residues in each domain, P1−P5, from *T. maritima*. The arrow shows the flow of phosphate within CheA.

and the rest of the protein by flexible linkers (*7*, *8*). The P3 domains from two CheA molecules come together to form a four-helix bundle, mediating dimerization. P4 is the catalytic domain responsible for ATP-binding and phosphotransfer to P1. The P5 domain binds CheW and regulates the autokinase rate in response to bound receptors (*9*, *10*).

P1 folds as five α helices (A−E), forming a four-helix-bundle motif common to histidine phosphotransferase domains, with the C-terminal fifth helix (E) packing against it (*11*, *12*). The conserved phosphoaccepting histidine (residue 45 in *Thermotoga maritima*) is located in helix B and is "activated" by a conserved hydrogen-bonding network, which forces it into the normally unfavored $N^{\delta 1}H$ tautomeric form (*13*, *14*).

The catalytic domain, P4, of CheA shows structural similarity to the functionally divergent GHL family of ATPases (*2*, *6*). P4 and the GHL ATPases share many common features, including a common fold, ATP-binding pocket, and four areas of conserved sequence, denoted the N, G1, F, and G2 boxes (*15*). While the GHL ATPase proteins essentially transfer the γ-phosporyl group of ATP to water, P4 instead transfers it to the reactive histidine on P1. To mitigate ATP hydrolysis, P4 lacks a catalytically essential glutamate residue found in the GHL ATPases. Instead, this glutamate may be provided by P1 along with the histidine phosphoacceptor (*6*, *14*).

The method by which CheA autophosphorylation activity is modulated in receptor−CheW−CheA complexes is currently a matter of debate. Here, we report progress toward discerning the mechanism of CheA regulation, using nuclear magnetic resonance (NMR) methods to monitor the interactions between CheA fragments P1 and P3P4 from the organism *T. maritima*. In addition, we have characterized two point mutations at the interaction surface suggested by the NMR data. These results suggest that the P1 domain is held in a conformation with H45 exposed and in a position to either accept a phosphate from ATP or to transfer the phosphate to CheY or CheB.

EXPERIMENTAL PROCEDURES

Protein Cloning, Expression, and Purification. T. maritima CheA fragments P1 (1−131), P4 (355−540), and P3P4 (290−540) were subcloned into vector pET22b (Novagen). The *Nde*1 and *Xho*1 restriction sites in pET22b were used, resulting in constructs with C-terminal histidine tags. The P3P4P5 (CheAΔ289) construct was received from Brian Crane (*6*). All plasmids were transformed and expressed in *Escherichia coli* strain BL21(DE3) (Novagen). For isotopically enriched samples, cells were grown in M9 minimal medium containing 1 g/L $^{15}NH_4Cl$ and 2 g/L ^{13}C or ^{12}C glucose, in D_2O or H_2O depending upon the protein sample made. Mutations P1-D93A and P3P4-E387A were introduced using the QuikChange site-directed mutagenesis kit (Stratagene). Protein purification was achieved by heat treatment (75 °C for 10 min) and centrifugation, followed by affinity chromatography of the supernatant on nickel−nitrilotriacetic acid beads (Qiagen). Samples were dialyzed into 50 mM Na_2HPO_4, 50 mM NaCl, and 0.04% sodium azide at pH 7.40, unless otherwise stated. All NMR samples contained 10% (v/v) ^2H_2O.

NMR Spectroscopy. NMR experiments were performed at 50 °C on a 600 MHz Varian spectrometer equipped with a $^1H[^{13}C/^{15}N]$ pulsed-field gradient probe unless stated otherwise. Sequential assignments of P1 and P4 were accomplished with ^1H-, ^{15}N-, and ^{13}C-labeled samples, using 3D, triple-resonance HNCACB and CBCA(CO)NH experiments (*16*−*18*). Heteronuclear single-quantum coherence (HSQC), HNCA, and HN(CO)CA transverse relaxation optimized spectroscopy (TROSY) spectra of P3P4 were recorded using a ^2H-, ^{15}N-, and ^{13}C-labeled sample at 45 °C on an 800 MHz Varian spectrometer with a cryoprobe (*19*−*21*). The lower temperature was necessary because of limitations associated with high-temperature operation over multi-day experimental runs of the cold probe. The titration experiments were performed as follows. Two 500 μL samples were prepared. Sample A contained 400 μM ^2H- and ^{15}N-labeled P1. Sample B contained 400 μM ^2H- and ^{15}N-labeled P1 and 1 mM unlabeled P3P4. These samples represent the titration endpoints, with molar ratios of 1.0:0.0 and 1.0:2.5 P1/P3P4, respectively. Samples with intermediate molar ratios were obtained by simultaneously transferring equal volumes from sample A to B and vice versa. All titrations were done in this manner, because it allows for the total concentration of the monitored species to remain unchanged. In the complementary titration, we monitored 400 μM ^2H- and ^{15}N-labeled P3P4 combined with varying concentrations of unlabeled P1 between 0 and 1 mM. A third titration was performed to monitor 216 μM ^1H- and ^{15}N-labeled P1-D93A combined with varying concentrations of unlabeled P3P4 between 0 and 796 μM. In all titrations, TROSY−HSQC spectra were recorded at each titration point. The sample used to monitor the P1−P3P4 interaction in the presence of the nucleotide and Mg^{+2} contained 400 μM ^2H- and ^{15}N-labeled P1 and 600 μM unlabeled P3P4 with (5′-adenyl(β,γ-methylene)-diphosphonate (ADPCP) and $MgCl_2$ added to a final concentration of 10 mM. All spectra were processed using the NMRPipe software package and analyzed using ANSIG (*22*, *23*).

Phosphorylation Assays. Initial velocities were measured for P1 and P1-D93A (0.05−1.5 mM) incubated with P3P4 (1 μM) or P3P4-E387A (1 μM). Buffer conditions were 50 mM hydroxymethylaminoethane (Tris) at pH 8.0 and 50 °C, 50 mM KCl, 20 mM $MgCl_2$, and 5 mM dithiothreitol (DTT). Samples were equilibrated to 50 °C, and then the reaction was initiated by the addition of an ATP and [γ-^{32}P]ATP mixture to a final concentration of 2 mM. At time intervals between 20 s and 2 h, aliquots were quenched with 2% sodium dodecyl sulfate (SDS) electrophoresis buffer containing 50 mM ethylenediaminetetraacetic acid (EDTA) and 10 mM cold ATP. Samples were then electrophoresed on 15% polyacrylamide gels. After electrophoresis, gels were immediately phosphorylation-quantified on a Storm phosphorimager (Amersham Biosciences).

Fluorescence Assays. P1 and P1-D93A proteins [modified with a $(His)_6$−Cys tag], at 150 μM concentration, were labeled with fluorescein-5-maleimide (F-5-M) as previously

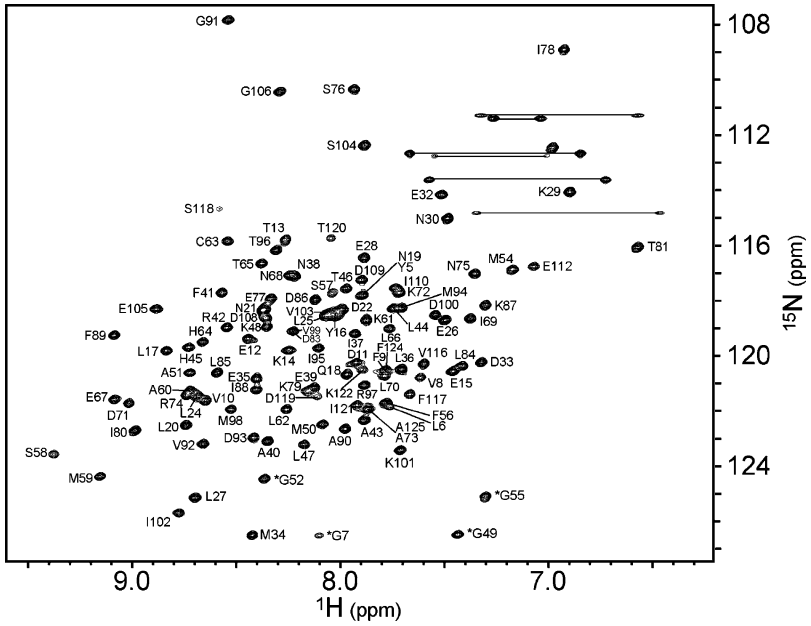

FIGURE 2: ^{1}H-^{15}N correlation map (HSQC) of uniformly ^{15}N-labeled CheA domain P1 from *T. maritima* at 50 °C and pH 7.4. The assignments of backbone amide protons are indicated. Asterisks indicate aliasing of the peaks from outside the spectral window along the ^{15}N dimension.

described (*24*). Fluorescence quenching assays were carried out on a Varian Cary Eclipse Fluorimeter. The excitation and emission wavelengths were 492 and 515 nm, respectively, using a slit width of 5 nm. Samples were maintained at 21 °C in a thermostated cuvette holder. Buffer conditions were 50 mM Tris at pH 8.0 and 21 °C, 50 mM KCl, 20 mM $MgCl_2$, and 1 mM DTT. Aliquots of a 1 mL 1 mM P3P4 plus 1 μM F-5-M*P1 or F-5-M*P1-D93A sample were exchanged with a 1 mL 1 μM F-5-M*P1 or F-5-M*P1-D93A sample, respectively. After each exchange, fluorescence intensity was measured and subsequently plotted as a function of the P3P4 concentration. Each resulting binding isotherm was fit to determine the respective dissociation constant. A titration of the dye, F-5-M, with P3P4 showed nonspecific dye binding to P3P4 with a K_d of ~1 mM. Therefore, it was necessary to account for protein and dye binding in the fitting of the binding isotherms. As a control, F-5-M*P1 was titrated with chicken egg white lysozyme. No quenching was detected.

RESULTS

NMR studies of CheA have been quite successful because of the modular architecture of the protein and the ability to experiment on single-domain constructs. To study the autophosphorylation interaction of CheA, domains P1 (15 kDa) and P4 (22 kDa) are necessary because they contain the phosphoaccepting histidine and the ATP-binding site, respectively. We initially chose to assign constructs of these two domains because of their tractable sizes and because of the high-quality NMR spectra that they give. However, as previously reported, P4 alone phosphorylates P1 more than 1000 times slower compared to a dimeric P3P4P5 construct (*25*). Our P3P4 construct, lacking the P5 domain, showed phosphorylation characteristics similar to P3P4P5, indicating that constructs, which minimally contain P3 and P4, are sufficient to effectively phosphorylate P1. Therefore, the assignments for the P4 construct were used to partially assign the larger, dimeric construct, P3P4.

Chemical-Shift Assignments. We have assigned the backbone resonances for 119 of the 130 nonproline backbone amides for P1. The assignments were made using the standard HNCACB and CBCA(CO)NH experiments. Figure 2 displays the assigned ^{1}H-^{15}N HSQC spectrum of P1. A total of 11 resonances are missing from the HSQC spectrum taken at 50 °C, most likely because of exchange broadening. These include S82, S107, five residues at the C terminus of P1, and four residues at the N terminus of P1. This dynamic behavior of the C-terminal region might reflect the fact that the P1 domain from *T. maritima* would not crystallize without the removal of the C-terminal helix (*26*). The four N-terminal residues exhibited sharp resonances at 25 but not at 50 °C as shown here, suggesting that the increased broadening is due to faster hydrogen-exchange rates for these residues at higher temperatures. The resonance of S118 is broadened but detectable. Otherwise, P1 has a well-dispersed H−N spectrum with sharp line widths and minimal peak overlap.

The P4 construct was assigned using the same assignment strategy as P1. Nearly complete assignments were obtained for P4 alone, except for approximately 20 sequential residues, from 489 to 511. The resonances from residues 489 to 511 appear to be exchange-broadened because of the flexibility of the "ATP-lid" associated with the active site of P4.

The ^{1}H-^{15}N spectrum of a ^{2}H- and ^{15}N-labeled P3P4P5 (90 kDa dimer) sample showed no resolved resonances at 50 °C (data not shown). To account for the extreme line broadening seen for this construct, we consider it likely that, in addition to the high molecular weight, the P5 domains of different dimers transiently associate, thus decreasing the effective molecular tumbling rate. This conclusion is based on the P5−P5 crystal contacts seen in the P3P4P5 crystal structure (*6*). Because P3P4P5 was intractable, backbone amide assignments of the P3P4 construct (57 kDa dimer) were derived from the assignments of isolated P4 combined with complimentary spectra from the P3P4 construct. The ^{1}H-^{15}N spectrum of isolated P4 correlates well with the

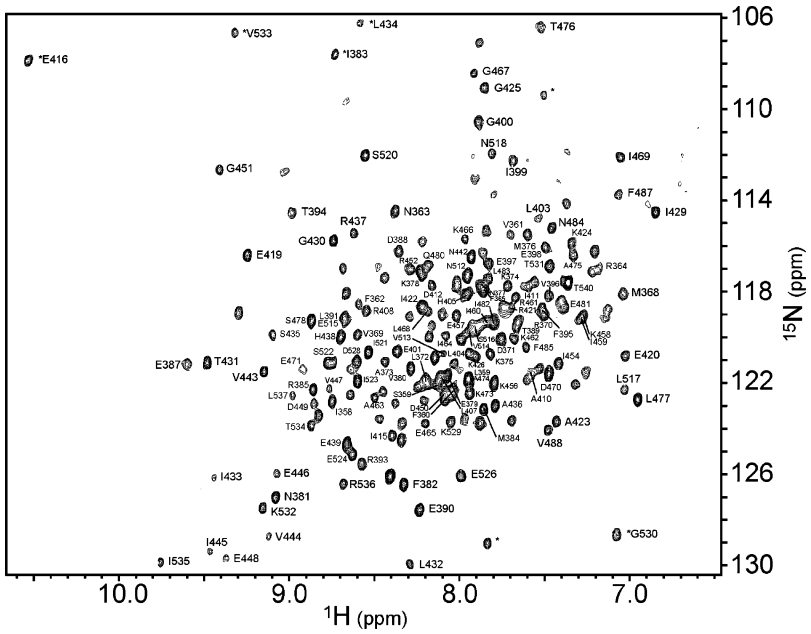

FIGURE 3: ^{1}H-^{15}N correlation map (TROSY−HSQC) of uniformly ^{15}N-labeled CheA construct P3P4 from *T. maritima* at 50 °C and pH 7.4. The assignments of backbone amide protons are indicated. Asterisks indicate aliasing of the peaks from outside the spectral window along the ^{15}N dimension.

spectrum from P3P4, allowing for assignment of the majority of P4 residues in P3P4. HNCA and HN(CO)CA TROSY spectra of ^{2}H-, ^{15}N-, and ^{13}C-labeled P3P4, taken at 800 MHz, were used to verify these assignments by comparing the CA-(i) and CA(i − 1) resonances from the two proteins. Figure 3 displays the assigned ^{1}H-^{15}N correlation spectrum of P3P4. Approximately 50 resonances are left unassigned in the P3P4 spectrum because no reliable sequential correlations could be established for them. We were able to reliably assign 135 of the 178 nonproline P4 resonances in P3P4 or 76%. Almost half of the unassigned residues make up the dynamic "ATP-lid" structure that could not be assigned in the P4 construct alone and did not show density in most of the published crystal structures, presumably because of the same disorder that causes line broadening here (*6*, *25*). The other half is found randomly throughout the sequence. Exclusion of the "ATP-lid", the portion of assignments transferred from P4 to P3P4 goes up to 85%, making this a reasonable approach to assign sections of larger multidomain proteins that would normally not be amenable to NMR assignment. The isolated P3 domain gave poor spectra, and no sequential correlations could be established in P3 or P3P4.

Although most P4 resonances were clearly identifiable in P3P4 from an overlay of the spectra from the two proteins, clear differences in the chemical shift were seen for some residues. Figure 4A charts the chemical-shift difference, for each assigned residue in P4, between the P4 and P3P4 constructs. Notably, several residues at the P3−P4 interface showed significant movement in peak position, with R393 and L403 having the largest change of ∼87 Hz each. When mapped onto the structure (Figure 4B), these changes appear to propagate from the interface through helix R392−D412 toward the other side of the structure, encroaching on the ATP-binding site. Such differences between P4 and P3P4 involving the hinge region at the P3−P4 interface may explain the kinase activity difference between the two constructs. However, considering the small differences overall in P4-residue chemical shifts in P4 versus P3P4, we conclude that there is minimal direct physical interaction between P3 and P4 in solution, consistent with their positions in the crystal structure (*6*).

Chemical-Shift-Perturbation Mapping of the P1−P3P4 Interaction. To better understand the regulation mechanism of CheA autophosphorylation, NMR-monitored titrations were carried out to observe interactions between P1 and P3P4 in vitro. Spectra were recorded using ^{2}H- and ^{15}N-labeled P1 in combination with unlabeled P3P4 or with ^{2}H- and ^{15}N-labeled P3P4 in combination with unlabeled P1 to view both sides of the interaction. The binding kinetics of P1 to P3P4 is such that the line broadening is in the fast exchange regime as evidenced by the population-weighted displacement of the peaks from free to bound states during the titration (Figure 5B). In both titrations, at >80% bound, line broadening because of increased molecular size made accurate peak positions difficult to define for some residues. Therefore, the chemical-shift changes presented here represent the difference in the chemical shift between free protein and a partially bound sample that provided accurate peak positions for all residues.

Significant chemical-shift changes were observed in several areas of P1 because of the binding to P3P4. Figure 5A shows the magnitude of the chemical-shift change, for each assigned residue of P1. The biggest changes were seen in residues G91−M98 at the center of helix D, with D93 having the largest change. Changes were also seen in residues D22−D25 of helix A and for the turn regions joining helices A and B and helices B and C near the top and bottom of the helix bundle, respectively. The only significant changes near the phosphorylation site, H45, came from residues G49, M50, and M54, near the turn region joining helices B and C, and were at approximately half of the magnitude as seen for G91−M98 (Figure 5A). These features are shown in a ribbon diagram of the crystal structure of P1 from *T. maritima*, with the chemical-shift changes coded by a color gradient (Figure 5C). Helix E residues (not shown in Figure 5C) showed relatively minor chemical-shift changes. Previous studies

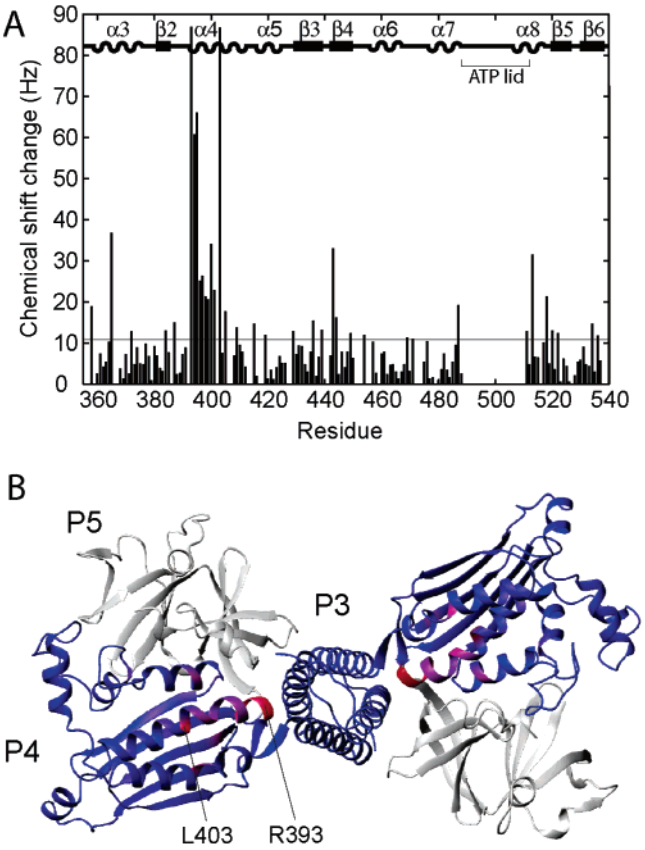

FIGURE 4: (A) Measured chemical-shift changes plotted by the residue number for CheA domain P4, for P4 versus P3P4 constructs, represented as $(\Delta H^2 + \Delta N^2)^{1/2}$ in hertz. Approximate locations of P4 secondary-structural elements are shown at the top. The horizontal gray line at 11.00 Hz denotes the average combined change in the ^{1}H and ^{15}N chemical shift. (B) Chemical-shift changes in CheA domain P4 residues, for P4 versus P3P4 constructs, are mapped onto a ribbon diagram of the P3P4P5 homodimer. A color gradient from blue to red indicates a 0−87 Hz change in chemical shift, and residues with the largest changes are labeled. The P5 domain is shown in gray.

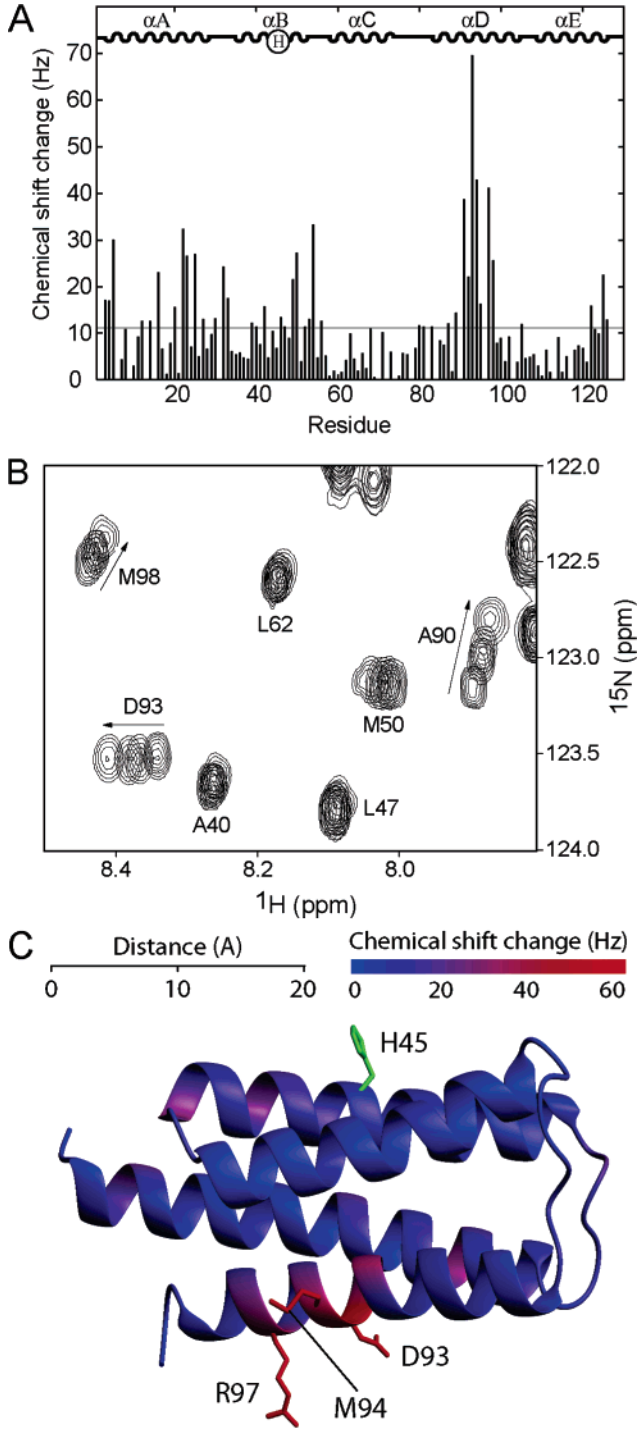

FIGURE 5: (A) Measured chemical-shift changes plotted by the residue number for CheA domain P1 upon binding P3P4, represented as $(\Delta H^2 + \Delta N^2)^{1/2}$ in hertz. Approximate locations of P1 secondary-structural elements and the phosphoreactive histidine are shown at the top. The horizontal gray line at 11.29 Hz denotes the average combined change in the ^{1}H and ^{15}N chemical shift. (B) Superimposed spectra of P1 combined with increasing amounts of P3P4. The spectral region shown highlights the larger shifts, indicated by arrows, seen in helix D (residues 90, 93, and 98) relative to helices B and C (residues 40, 47, 50, and 62). (C) Chemical-shift changes in P1 because of the binding of P3P4 mapped onto a ribbon diagram. The residues with the three largest chemical-shift changes and the phosphoaccepting histidine are labeled. A color gradient from blue to red indicates a 0−60 Hz change, and a 20 Å ruler is shown for reference. Because the crystal structure of P1 from *T. maritima* contains only the first four of five helices (A−D), only the data for residues 1−104 are shown (*26*).

have shown that a truncated P1 construct lacking helix E functions similarly to wild-type (WT) P1, suggesting that helix E is not necessary for CheA autophosphorylation (*14*). The titration data presented here indicate that helix E is also not involved in direct interaction with P3P4. Interestingly, the most affected residues from binding were not located in helix B, in the vicinity of H45, but were located on a different surface from where H45 resides. This result raises the question of whether this binding mode is related to catalysis?

Notably, these experiments were carried out in the absence of Mg^{+2} and ATP. Because both are required for catalysis, it is reasonable to suggest that these ligands may be necessary for P1 and P3P4 to adopt a catalytically productive binding mode. To test their effect on the P1−P3P4 interaction, $MgCl_2$ and a nonhydrolyzable ATP analogue, ADPCP, were added to a ^{2}H- and ^{15}N-labeled P1 sample bound to unlabeled P3P4. No changes were seen in the chemical-shift changes of P1 upon binding P3P4.

To clarify the P1−P3P4 interaction, we also performed chemical-shift-perturbation mapping of ^{2}H- and ^{15}N-labeled P3P4 by titrating unlabeled P1. Figure 6 shows the chemical-shift changes in P3P4 upon binding P1 for each assigned residue of P3P4. Clearly, most of the changes happen between residues 360 and 410, roughly the N-terminal third

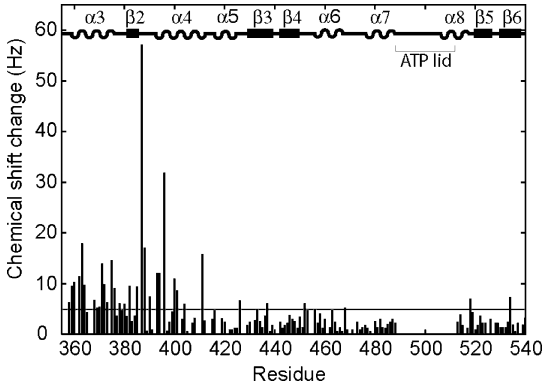

FIGURE 6: Measured chemical-shift changes plotted by the residue number for CheA construct P3P4 upon binding P1, represented as $(\Delta H^2 + \Delta N^2)^{1/2}$ in hertz. Approximate locations of P4 secondary-structural elements and the "ATP-lid" region are shown at the top. The horizontal gray line at 4.58 Hz denotes the average combined change in the ^{1}H and ^{15}N chemical shift.

of P3P4. When these changes were placed onto the CheA structure in a color-coded representation (Figure 7), we were interested to learn that the bulk of perturbed residues were far from the P4 active site. The residues showing the largest chemical-shift changes, E387 and V396, are 27 and 21 Å, respectively, from the position of the ATP γ-phosphoryl group in the same monomer and even further from the ATP-binding site of the other monomer in the crystal dimer structure (*25*).

The perturbed residues in P3P4 appear to be split into two groups: a large, primary group near E387 and a small, secondary group bordering the ATP pocket. The primary group, with the largest chemical-shift changes from N363, E387, D388, and V396, cluster near the P3−P4 interface, approximately 25 Å from the ATP-binding site. These residues have chemical-shift changes in the 15−60 Hz range. This cluster also contains residues F360, V361, F362, R393, and T394, with chemical-shift changes between 10 and 15 Hz. The secondary cluster, made up of D371, K375, and I411, is much closer to the ATP-binding site and has chemical-shift changes in the 13−16 Hz range. This smaller cluster is likely related to secondary-structural changes resulting from direct binding at the primary site near the P3−P4 interface. This conclusion is supported by the evidence discussed above that changes at the P3−P4 hinge region resulting from the covalent attachment of P3−P4 led to long-range changes propagating toward the other side of the structure, similar to what we see with P1 binding.

It should be noted that binding of P1−P3 and the linker region joining P3 and P4 could not be directly analyzed because of the absence of assignments. However, resonances from these regions are identified by their presence in the P3P4 spectrum and absence or significant displacement in the P4 spectrum. Among the unassigned resonances clearly contributed by P3 or the linker, several peaks showed chemical-shift changes in the 10−20 Hz range upon binding P1, and none have shifted more than half the magnitude of the largest changes observed for the residues in the primary cluster. Because the residues in P3P4 displaying the largest shifts are proximal to P3, it is likely that the P3−P4 linker and several C-terminal residues in P3 are involved in or affected by binding.

Mutational Analysis. In an attempt to clarify the significance of these data, alanine replacements were constructed at the residues with the largest shift in P1-D93A and P3P4-E387A. The initial rates were determined from phosphorylation assays and used to calculate K_m values for the WT and mutant proteins. The values obtained are listed in Table 1. The K_m value of P1-WT/P3P4-WT, at 50 °C, agrees closely with the published K_m value of 270 μM at 50 °C (*26*). Significant changes in the K_m value were not seen for the mutants. However, the rate of P1-D93A phosphorylation was an order of magnitude slower than P1-WT. This is apparently a V_{max} effect. Therefore, we propose that P1-residue D93 is important to either the P1 structure or P3P4-binding even though it resides on the opposite surface from H45. The phosphorylation rate of P3P4-E387A was twice as fast as P3P4-WT in phosphorylating either P1-WT or P1-D93A. However, the significance of this modest change is not clear.

The effect of the D93A mutation on the ^{1}H-^{15}N HSQC spectrum of P1 was substantial but localized. Residues 89−98 in helix D all displayed combined amide ^{1}H- and ^{15}N-shift changes in the 30−80 Hz range. Residues 24, 59, 66, 99, 104, 109, 117, and 121 had smaller chemical-shift changes in the 12−20 Hz range. All of these residues reside in helices A, D, and E, except residues 59 and 66, which are in helix C but orient into the protein core toward helix D. The peak positions for all other residues in helices B and C, including H45, were essentially unchanged (0−6 Hz). We performed chemical-shift-perturbation mapping of ^{1}H- and ^{15}N-labeled P1-D93A by titrating unlabeled P3P4. The chemical-shift changes seen in helix D of P1, for the P1/P3P4 interaction, were absent in this interaction. Interestingly, the chemical-shift changes seen near the turn region between helices B and C were still present (data not shown).

Fluorescence quenching experiments were also carried out on fluorescein-tagged versions of the mutant and WT proteins. The dissociation constants (K_d) at 21 °C are listed in Table 1. Because of the large difference in experimental temperature, no conclusions should be drawn concerning the differences in K_d and K_m values. No quenching was detected in the fluorescence experiment on P3P4-E387A; however, this should not be interpreted as the absence of binding. A titration of ^{2}H- and ^{15}N-labeled P1 with unlabeled P3P4-E387A showed chemical-shift changes equivalent to those seen with P3P4-WT.

DISCUSSION

The primary P1 interaction surface of P3P4 identified in this study consists mainly of residues near or at the P3−P4 interface. The involvement of P3 and P4 residues near the linker region in binding P1 seems likely, supported by the fact that P1 binding is only observable by NMR with P3P4 but not P3 or P4 alone (data not shown). P1 binding to this area also places P1 close to the symmetric dimer interface, increasing the possibility of P1 interacting uniquely with each P3P4 monomer in the dimer. Additionally, it is plausible that, in P3P4, P4 may adopt a quaternary structure relative to P3 that is different from that seen in the crystal structure. If so, the interaction between P3 and P4 may change in the presence of P1, contributing to the chemical-shift changes seen.

The line broadening of the "ATP-lid" resonances obscures any binding of P1 to the ATP-lid region, thus masking

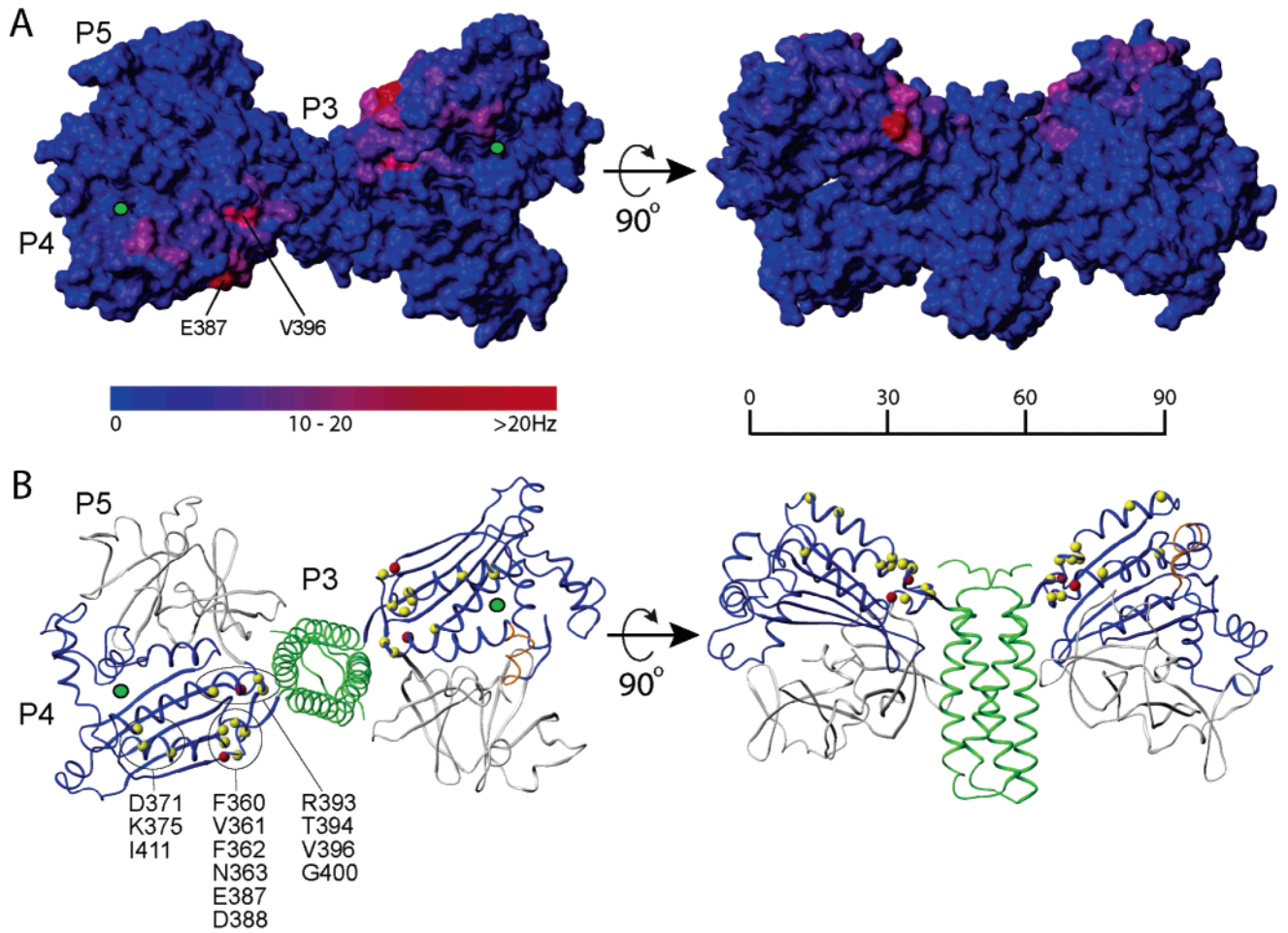

FIGURE 7: (A) Chemical-shift changes in P3P4 upon binding P1 mapped onto a molecular surface representation of P3P4P5. The two views are rotated 90° about the *x* axis. The positions of each domain and residues E387 and V396 are labeled. Green dots represent the approximate location of the ATP-binding pocket. A color gradient from blue to red has been applied to the P4 domain only, indicating a 0−20 Hz change. Numbers above the ruler correspond to distances in angstroms. (B) Ribbon diagram showing the positions of residues, with the largest chemical-shift changes in P3P4 upon binding P1. The residues with the greatest chemical-shift changes are shown as yellow balls, with E387 and V396 colored in red. The P3 domain is colored green, and P5 is colored gray. The ATP-lid region is colored orange on one monomer.

Table 1: Kinetic Data Describing the Phosphorylation Reaction of Variants of P1 and P3P4 at 50 °C[a]

P1 variant	P3P4 variant	K_d (μM)	K_m (μM)	V_{max} (min^{-1})
P1	P3P4	23 ± 5.1	239 ± 37	35.5 ± 1.7
P1-D93A	P3P4	20.3 ± 6.8	434 ± 145	3.5 ± 0.5
P1	P3P4-E387A	undetectable	183 ± 57	68.2 ± 5.7
P1-D93A	P3P4-E387A		545 ± 117	5.5 ± 0.5

[a] K_d values are from fluorescence quenching experiments, recorded at 21°C.

possible details of the P3P4 interaction with P1. Although it is necessary to consider the possibility of P1 binding to the ATP-lid, we find this situation highly unlikely. The resonances of residues corresponding to the ATP-lid are broadened because of their dynamic nature, and an interaction with P1 would likely ameliorate this movement, resulting in reduced line broadening. Tellingly, no new resonances appeared throughout the course of the P3P4 titration with P1, suggesting that the ATP-lid resonances remained broadened.

The P3P4 interaction surface of P1 suggested by our chemical-shift-perturbation mapping experiments is opposite to the surface containing the phosphorylation site H45. In experiments of this kind, the surface showing the largest chemical-shift perturbations is often involved directly in binding. However, the high-resolution crystal structure of P1 from *T. maritima* shows two forms of helices A and D relative to the remainder of the protein. If P1 binding to P3P4 were to "lock" P1 into one of these two forms, some chemical-shift changes may be expected. Therefore, while our results must be tempered by the possibility of a conformational change causing the largest shifts in helix D, the absence of chemical-shift changes of a similar magnitude proximal to H45 suggest that binding involving helices B and C is weak at best.

Docking of P1 and P3P4 via their suggested interaction surfaces orients the P1 surface containing H45 at least 20 Å away from the ATP sites of both subunits in the bound P3P4 dimer. The long distance between the H45 in P1 and the ATP-binding sites in P3P4 prevents the direct interaction between these sites both within and between the subunits. However, for catalysis to occur, productive docking of P1 and P3P4 would necessarily bring the P1 phosphoaccepting histidine into the proximity of the γ-phosphoryl group of a P3P4-bound ATP molecule. If this suggested binding mode is productive for catalysis, large-scale motions are required to bring together the active sites of P4 and P1. Alternatively,

the binding mode observed here may play a role in the regulation of the kinase activity rather than in catalysis involving the transfer of the phosphate from ATP.

If this binding mode is involved in catalysis, we need to consider that CheA exists predominantly as a dimer. Surette et al. have shown that isolated CheA from *E. coli* exists in an equilibrium of active dimers and inactive monomers (*27*). Therefore, in *E. coli* CheA, dimerization through the P3 domains is required for activation. A recent crystal structure of the entire dimeric, cytoplasmic fragment of a putative histidine kinase (*28*) led the researchers to favor a mechanism whereby the kinase domain from one dimer partner reorients to a position capable of transphosphorylating the reactive histidine of the other dimer partner. In their system as well as most other histidine kinases, the reactive histidine is located on the dimerization domain, equivalent to P3 here. CheA has evolved a separate phosphorelay domain, P1; however, we consider that CheA may try to mimic these other kinases by orienting the reactive histidine near the P3 domain for phosphorylation to occur. If this model is correct and conserved in CheA, then large-scale, hinged P3−P4 motions are required. It has been previously speculated that, because of the limited interactions between the P3 and P4 domains and the conservation of the hinge region attaching them, movement of these domains may be an essential characteristic of histidine kinase signaling (*6*). In the fast exchange limit, as seen here, P1 could interact differently with each monomer in a P3P4 dimer and we would still observe a single time-averaged peak position of P1 resonances in our NMR data.

For a possible regulatory role of this binding mode, we speculate that CheA could be regulated by sequestering P1 away from the P4 active site. Because P1 and P4 reside in the same molecular complex, their molar ratio is 1:1 and CheA could mediate access to a productive site by exclusively modulating the affinity of an unproductive site for P1. CheA alone has an autophosphorylation rate 1000-fold lower than in receptor complexes. Without the proper cofactors, CheA may assume an inactive conformation, which includes a relatively high-affinity, unproductive P1-binding site. The chemical-shift perturbations seen here could reflect this unproductive site or a combination of multiple sites.

Another possible role of this binding mode is to regulate CheY access to phosphorylated P1. Minimally, the P1 domain must sample two binding modes to first become phosphorylated by P4 and then transfer this phosphate to CheY. In the latter state, the P1 phosphoaccepting histidine needs to be accessible to CheY. In NMR spectra of full-length CheA from *E. coli*, the only sharp resonances observed correspond to residues in the P2 domain, even in the presence of ATP (data not shown). The resonances corresponding to the P3P4P5 region of CheA are expected to be broadened, because of the larger size of the region and therefore slower rotational correlation time. Clearly, the P2 resonances are sharp because the flexible linkers allow for the rotation of P2 to be uncorrelated with the remainder of the protein. Contrary to P2, the observed broadening of the P1 resonances in full-length CheA suggests that P1 is bound to P3P4P5, even when phosphorylated. This fact hints that CheY may access P1 for phosphotransfer while P1 is bound to P3P4P5. Our results describe a complex between P1 and P3P4 that would sterically allow CheY access to the P1-phosphoaccepting histidine.

The phosphorylation kinetics of the P1-D93A and P3P4-E387A mutants versus WT P1 are interesting. The most significant change was the 10-fold decrease in the V_{max} of the P1-D93A mutant; however, fluorescence quenching assays showed that this mutant bound P3P4 with the same affinity as P1-WT. The fact that the binding affinity observed was not affected while the phosphorylation rate was suggests two possibilities. The D93A mutation could intrinsically affect the ability of P1 to be phosphorylated, without affecting the interaction between P1 and P3P4, or the binding event that we are observing may not be the event that leads to phosphorylation. The absence of chemical-shift differences between P1-WT and P1-D93A for residues near H45 indicates no change in the local structure near the site of phosphorylation and argues for the latter possibility.

The chemical-shift changes seen in P1-D93A upon interacting with P3P4 are of interest. No chemical-shift changes larger than 12 Hz were seen in helix D. However, the turn region between helices B and C had changes in the 20−30 Hz range, similar to those seen in P1-WT upon the interaction with P3P4. While it is tempting to speculate on the meaning of these data, the shifts seen are small and further studies are needed to ascertain whether this region is directly involved in binding P3P4. While a mechanism involving multiple P1-binding orientations or sites per P3P4 monomer is speculative, it does help explain our findings. Overall, the results presented here raise a number of important questions. Further research into the role of the P3 domain in activating P4 and the positioning of the P1 domain relative to P4 is underway.

REFERENCES

1. Stock, A. M., Robinson, V. L., and Goudreau, P. N. (2000) Two-component signal transduction, *Annu. Rev. Biochem. 69*, 183−215.
2. Parkinson, J. S., and Kofoid, E. C. (1992) Communication modules in bacterial signaling proteins, *Annu. Rev. Genet. 26*, 71−112.
3. Falke, J. J., Bass, R. B., Butler, S. L., Chervitz, S. A., and Danielson, M. A. (1997) The two-component signaling pathway of bacterial chemotaxis: A molecular view of signal transduction by receptors, kinases, and adaptation enzymes, *Annu. Rev. Cell Dev. Biol. 13*, 457−512.
4. Perego M. (1998) Kinase-phosphatase competition regulates *Bacillus subtilis* development, *Trends Microbiol. 6*, 366−370.
5. Marques, R. R., and Carbonetti, N. H. (1997) Genetic analysis of pertussis toxin promoter activation in *Bordetella pertussis*, *Mol. Microbiol. 24*, 1215−1224.
6. Bilwes, A. M., Alex, L. A., Crane, B. R., and Simon, M. I. (1999) Structure of CheA, a signal-transducing histidine kinase, *Cell 96*, 131−141.
7. Zhou, H., McEvoy, M. M., Lowry, D. F., Swanson, R. V., Simon, M. I., and Dahlquist, F. W. (1996) Phosphotransfer and CheY-binding domains of the histidine autokinase CheA are joined by a flexible linker, *Biochemistry 35*, 433−443.
8. Morrison, T. B., and Parkinson, J. S. (1994) Liberation of an interaction domain from the phosphotransfer region of CheA, a signaling kinase of *Escherichia coli*, *Proc. Natl. Acad. Sci. U.S.A. 91*, 5485−5489.
9. Bourret, R. B., Davagnino, J., and Simon, M. I. (1993) The carboxy-terminal portion of the CheA kinase mediates regulation of autophosphorylation by transducer and CheW, *J. Bacteriol. 175*, 2097−2101.
10. Swanson, R. V., Schuster, S. C., and Simon, M. I. (1993) Expression of CheA fragments which define domains encoding kinase, phosphotransfer and CheY binding activities, *Biochemistry 32*, 7623−7629.

11. Zhou, H., Lowry, D. F., Swanson, R. V., Simon, M. I., and Dahlquist, F. W. (1995) NMR studies of the phosphotransfer domain of the histidine kinase CheA from *Escherichia coli*: Assignments, secondary structure, general fold, and backbone dynamics, *Biochemistry 34*, 13858−13870.
12. Mourey, L., Da Re, S., Pedelacq, J. D., Tolstykh, T., Faurie, C., Guillet, V., Stock, J. B., and Samama, J. P. (2001) Crystal structure of the CheA histidine phosphotransfer domain that mediates response regulator phosphorylation in bacterial chemotaxis, *J. Biol. Chem. 276*, 31074−31082.
13. Zhou, H., and Dahlquist, F. W. (1997) Phosphotransfer site of the chemotaxis-specific protein kinase CheA as revealed by NMR, *Biochemistry 36*, 699−710.
14. Quezada, C. M., Hamel, D. J., Gradinaru, C., Bilwes, A. M., Dahlquist, F. W., Crane, B. R., and Simon, M. I. (2005) Structural and chemical requirements for histidine phosphorylation by the chemotaxis kinase CheA, *J. Biol. Chem. 280*, 30581−30585.
15. Alex, L. A., and Simon, M. I. (1994) Protein histidine kinases and signal transduction in prokaryotes and eukaryotes, *Trends Genet. 10*, 133−138.
16. Muhandiram, D. R., and Kay, L. E. (1994) Gradient-enhanced triple-resonance three-dimensional NMR experiments with improved sensitivity, *J. Magn. Reson. B 103*, 203−216.
17. Wittekind, M., and Mueller, L. (1993) HNCACB, a high-sensitivity 3D NMR experiment to correlate amide-proton and nitrogen resonances with the α- and *β*-carbon resonances in proteins, *J. Magn. Reson. B 101*, 201−205.
18. Grzesiek, S., and Bax, A. (1992) Correlating backbone amide and side chain resonances in larger proteins by multiple relayed triple resonance NMR, *J. Am. Chem. Soc. 114*, 6291−6293.
19. Pervushin, K., Riek, R., Wider, G., and Wuthrich, K. (1997) Attenuated T2 relaxation by mutual cancellation of dipole−dipole coupling and chemical shift anisotropy indicates an avenue to NMR structures of very large biological macromolecules in solution, *Proc. Natl. Acad. Sci. U.S.A. 94*, 12366−12371.
20. Yang, D. W., and Kay, L. E. (1999) Improved ^{1}HN-detected triple resonance TROSY-based experiments, *J. Biomol. NMR 13*, 3−10.
21. Yang, D. W., and Kay, L. E. (1999) TROSY triple-resonance four-dimensional NMR spectroscopy of a 46 ns tumbling protein, *J. Am. Chem. Soc. 121*, 2571−2575.
22. Delaglio, F., Grzesiek, S., Vuister, G. W., Zhu, G., Pfeifer, J., and Bax, A. (1995) NMRPipe: A multidimensional spectral processing system based on UNIX pipes, *J. Biomol. NMR. 6*, 277−293.
23. Kraulis, P. J. (1989) ANSIG: A program for the assignment of protein ^{1}H 2D NMR spectra by interactive graphics, *J. Magn. Reson. 84*, 627−633.
24. Boukhvalova, M. S., Dahlquist, F. W., and Stewart, R. C. (2002) CheW binding interactions with CheA and Tar. Importance for chemotaxis signaling in *Escherichia coli*, *J. Biol. Chem. 277*, 22251−22259.
25. Bilwes, A. M., Quezada, C. M., Croal, L. R., Crane, B. R., and Simon, M. I. (2001) Nucleotide binding by the histidine kinase CheA, *Nat. Struct. Biol. 8*, 353−360.
26. Quezada, C. M., Gradinaru, C., Simon, M. I., Bilwes, A. M., and Crane, B. R. (2004) Helical shifts generate two distinct conformers in the atomic resolution structure of the CheA phosphotransferase domain from *Thermotoga maritima*, *J. Mol. Biol. 341*, 1283−1294.
27. Surette, M. G., Levit, M., Liu, Y., Lukat, G., Ninfa, E. G., Ninfa, A., and Stock, J. B. (1996) Dimerization is required for the activity of the protein histidine kinase CheA that mediates signal transduction in bacterial chemotaxis, *J. Biol. Chem. 271*, 939−945.
28. Marina, A., Waldburger, C. D., and Hendrickson, W. A. (2005) Structure of the entire cytoplasmic portion of a sensor histidine-kinase protein, *EMBO J. 24*, 4247−4259.

BI060798K